Search for the non-resonant Higgs-pair production in $\ell^+\ell^-\ell^+\ell^-$ final state at $\sqrt{s} = 13$ TeV in the ATLAS detector

Abdualazem Fadol[1, 2], Yaquan Fang[2], Bruce Mellado[1] and Xifeng Ruan[1]

[1] School of Physics and Institute for Collider Particle Physics, University of the Witwatersrand, Johannesburg, Wits 2050, South Africa
[2] Institute of High Energy Physics, University of Chinese Academy of Sciences, 19B Yuquan Road, Shijingshan District, Beijing 100049, China

E-mail: amohammed@aims.ac.tz

Abstract. A search for the non-resonant production of a pair of the Standard Model Higgs boson h via gluon fusion, $gg \to hh$, is performed. Each Higgs boson decays to either $2W$, $2Z$ or 2τ, leading to $4\ell + X$ in the final state. The ℓ could be an electron or a muon, and X is missing transverse energy or jets. The search uses Monte Carlo samples at a centre-of-mass energy of 13 TeV generated according to the ATLAS detector configurations with an integrated luminosity of 139 fb^{-1}. The expected upper limit on the cross-section times the Standard Model (SM) Higgs pair branching ratio is found to be 49.22 times the SM prediction.

1. Introduction

A new era has emerged in High Energy Physics after the ATLAS [1] and CMS [2] experiments discovered a new scalar boson. Various measurements have been performed to confirm the compatibility of the new particle with the Higgs boson, h, which is predicted by the Standard Model (SM) [3, 4]. The SM predicted the existence of the non-resonant Higgs pair production and Higgs self-coupling. A search using 36.1 fb^{-1} datasets in the $hh \to WW^{(*)}WW^{(*)}$ showed no significant excess above the considered SM background is found [5]. However, the Higgs pair production is significantly enhanced by altering the Higgs boson self-coupling [6] or in extended Higgs sectors scenarios [7].

With the current 139 fb^{-1} dataset, one expects the sensitivity of the Higgs pair production to improve. In addition, including channels with a small branching ratio is expected to enhance the exploration. This study analyses the non-resonant Higgs pair production via gluon fusion, which subsequently decay to $4\ell(\ell = e,$ or $\mu)$ final state. Each of the two Higgs bosons decays to $2W$, $2Z$ or 2τ, leading to $4\ell + X$, where X could either be missing transverse energy or jets. The combination of the Higgs decay products is shown in Figure 1 with their branching fractions. There are nine possible permutations, namely— $4W$, $4Z$, 4τ, $2W2Z$, $2Z2W$, $2W2\tau$, $2\tau2W$, $2Z2\tau$ or $2\tau2Z$. About 25% of the hh events are expected to come from the $hh \to 4W$, 20% from $hh \to 2Z2W$, and 11% from $hh \to 2W2\tau$. Other hh events such as $hh \to 4Z$, $hh \to 4\tau$, and $hh \to 2Z2\tau$ are expected to be less than 10%. Only Monte Carlo (MC) simulations are used in the analysis for the signal optimisation with an integrated luminosity of 139 fb^{-1}.

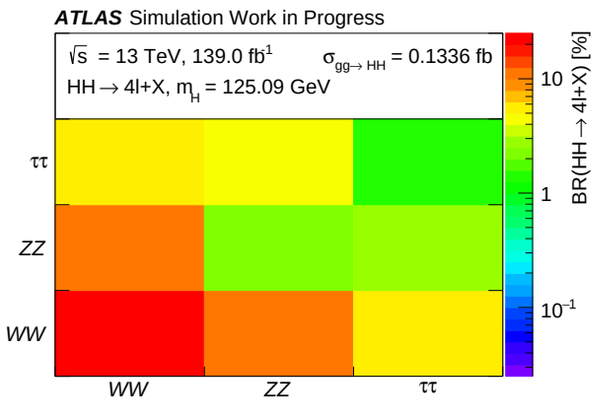

Figure 1. Di-Higgs decay modes and the calculated branching fraction of Di-Higgs to four leptons and X at the reconstruction level. The assumed Higss mass is 125.09 GeV and the Higgs pair production cross-section in gluon fusion is 0.1336 fb.

This paper is organised as follows, MC samples used in the analysis are described in section 2. The event selection and analysis strategy are explained in section 3 and section 4, respectively. Systematic uncertainties included in the analysis are discussed in section 5. Section 6 shows the statistical procedure, results and discussion. Finally, the conclusion is given in section 7.

2. Monte Carlo samples

MC simulation according to the ATLAS experiment configuration is used. The samples are generated in three campaigns to emulate the 2015 - 2016, 2017 and 2018 data taking periods. The combination of all campaigns together matches up to an integrated luminosity of 139 fb^{-1}. Non-resonant, $gg \to hh$, signal and $t\bar{t}V$ background samples are generated at NLO using MadGraph5_aMC@NLO [8] interfaced with Pythia 8 [9] for the hadronisation. Background processes such as $q\bar{q} \to ZZ$, $q\bar{q} \to ZZ$ (EW), $VVV(V = Z/W^{\pm})$ and Z+jets are simulated using Sherpa 2.2.2 [10] with NNPDF30NNLO [11] parton distribution function (PDF) set. The $t\bar{t}$ events were generated using Powheg-Box v2 [12] with NNPDF30NNLO PDF set. Pythia 8 was used as an interface for the showering and hadronisation with A14 NNPDF23LO tune, and EvtGen [13] was used to simulate B-hadron decays. Powheg-Box v2 and Pythia 8 were used for the generation and hadronisation of the WZ process.

3. Event selection

Electrons must be within the inner tracking detector system ($|\eta| < 2.47$ excluding the $1.37 < |\eta| < 1.52$ region) and have transverse energy $E_{\mathrm{T}} > 7$ GeV. Muons are required to be inside $|\eta| < 2.7$ scope of the muon spectrometer, and have transverse momentum $p_{\mathrm{T}} > 5$ GeV. Events are selected if they only contain exactly four leptons with $p_{\mathrm{T}}^{\ell} > 10$ GeV, and a total charge sum equal to zero. Events are required to pass single- and di-lepton trigger [14], and at least one of the lepton candidate need to be matched to the trigger. After choosing four isolated leptons, events are classified further according to the number of lepton pairs. Events must have two same-flavour and opposite charges (2-SFOS) lepton pairs such as $4e$, 4μ and $\mu 2e$. In addition to events with one or zero same-flavour opposite charges pairs (1-SFOS or 0-SFOS), for instance, $e\mu\mu\mu$ and $e\mu e\mu$. The 0-SFOS events are combined with 1-SFOS (0/1-SFOS) due to the low statistics. In each quadruplet, the p_{T} of the leading lepton has to be higher than the succeeding one. The quadruplets are selected based on matching the invariant mass of the second lepton pairs m_{Z_2} to be closest to the Z boson mass, and the first lepton pair were taken as m_{Z_1}. Events

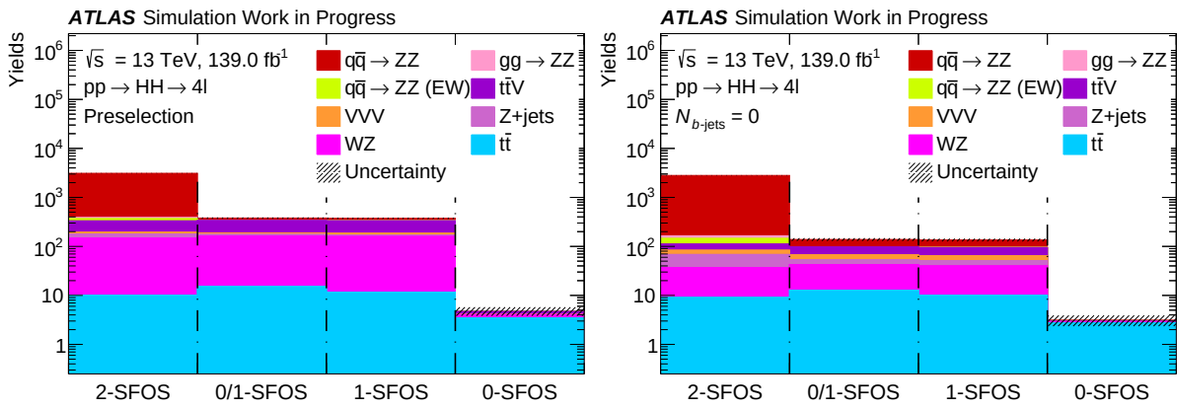

(a) (b)

Figure 2. The expected background yields for MC simulation after the (a) preselection and (b) $N_{b-\text{jets}} = 0$ for the 2-SFOS, 1-SFOS, 0/1-SFOS and 0-SFOS categories.

carrying one or more b-jets are vetoed to suppress top related backgrounds further. Figure 2 shows the yield for each background component with and without the b-jet veto for 2-SFOS, 1-SFOS, 0-SFOS, and 0/1-SFOS categories.

4. Analysis strategy

A boosted decision tree (BDT) based on the Multivariate analysis package (TMVA) [16] is used to separate the $hh \to 4\ell + X$ signal from the background. Events are divided equally into two sets; the first half is used for training the BDT algorithm. And the other half is employed to test the performance of the method. Table 1 shows the unweighted events of the signal and backgrounds for 0/1-SFOS and 2-SFOS categories after the b-veto.

Sixteen variables are used as inputs to the BDT, including the four leptons invariant mass. The correlation between features is shown in Figure 3. Some of the variables have a high correlation; for instance, the first lepton momentum is correlated with the scalar sum of leptons. Table 2 summarises the description of each variable, its ranking and the separation power. The best- and worst-ranked variable are labelled 1 and 16, respectively. The invariant mass of the second lepton pair has the best ranking in 0/1-SFOS, while the invariant mass of the first lepton

Table 1. Unweighted events for the signal and backgrounds component in each category used in the training and testing. Events are shown after vetoing the b-jets.

	0/1-SFOS	2-SFOS
$q\bar{q} \to ZZ$	21675	1528977
$q\bar{q} \to ZZ$ (EW)	375	28806
$gg \to ZZ$	2966	256910
$t\bar{t}V$	11031	10105
VVV	18467	57908
Z+jets	69	116
WZ	328	276
$t\bar{t}V$	92	68
$hh \to 4\ell + X$	4340	3781

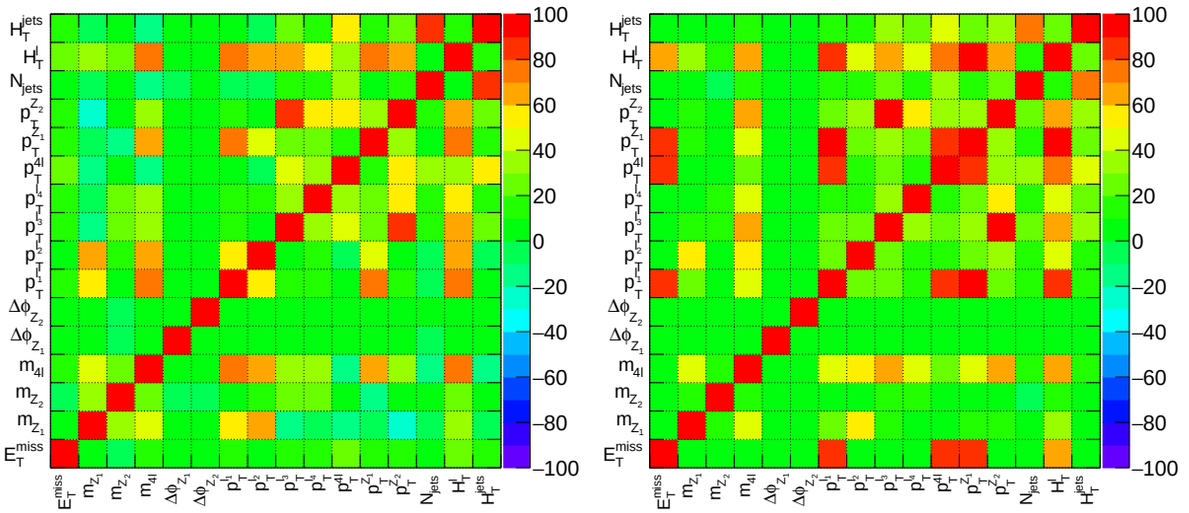

(a) Signal (b) Backgrounds

Figure 3. The correlation between input features for signal and background of the 2-SFOS category.

pair is the best in 2-SFOS. A comparison between BDT and other MVA methods is illustrated in Figure 4(a) for 2-SFOS. It shows that the Receiver operating characteristic (ROC) curve for the BDT is better. Figure 4(b) shows the ROC curve for the 0/1-SFOS and 2-SFOS categories.

Table 2. Input features used for the training and their ranking and separation power for 2-SFOS and 0/1-SFOS category. The higher the percentage value of the separation power, the better the ranking—the best-ranking start from 1 to the worst-ranked 16.

Input variable	Description	0/1-SFOS		2-SFOS	
		Rank	Separation	Rank	Separation
$E_{\mathrm{T}}^{\mathrm{miss}}$	Missing transverse energy	11	4.56%	2	37.82%
m_{Z_1}	Invariant mass of the first lepton pair	16	2.16%	1	52.44%
m_{Z_2}	Invariant mass of the second lepton pair	1	26.31%	4	30.88%
$m_{4\ell}$	Four-lepton invariant mass	4	6.10%	5	16.93%
$\Delta\phi_{Z_1}$	The azimuthal angle between the first lepton pair	2	11.52%	7	15.75%
$\Delta\phi_{Z_2}$	The azimuthal angle between the second lepton pair	6	5.73%	9	9.99%
$p_{\mathrm{T}}^{\ell_1}$	p_{T} of the first lepton	3	7.35%	12	5.36%
$p_{\mathrm{T}}^{\ell_2}$	p_{T} of the second lepton	8	5.16%	13	5.25%
$p_{\mathrm{T}}^{\ell_3}$	p_{T} of the third lepton	13	3.82%	15	3.74%
$p_{\mathrm{T}}^{\ell_4}$	p_{T} of fourth lepton	14	2.58%	10	6.17%
$p_{\mathrm{T}}^{4\ell}$	p_{T} of the four-lepton system	7	5.49%	3	31.66%
$p_{\mathrm{T}}^{Z_1}$	p_{T} of the first lepton pair	12	4.29%	16	3.02%
$p_{\mathrm{T}}^{Z_2}$	p_{T} of the second lepton pair	15	2.29%	11	6.11%
N_{jets}	Number of the jets	10	4.61%	8	15.05%
H_{T}^{ℓ}	Scalar sum of the leptons p_{T}	5	5.95%	14	4.41%
$H_{\mathrm{T}}^{\mathrm{jets}}$	Scalar sum of the jets p_{T}	9	2.16%	6	16.92%

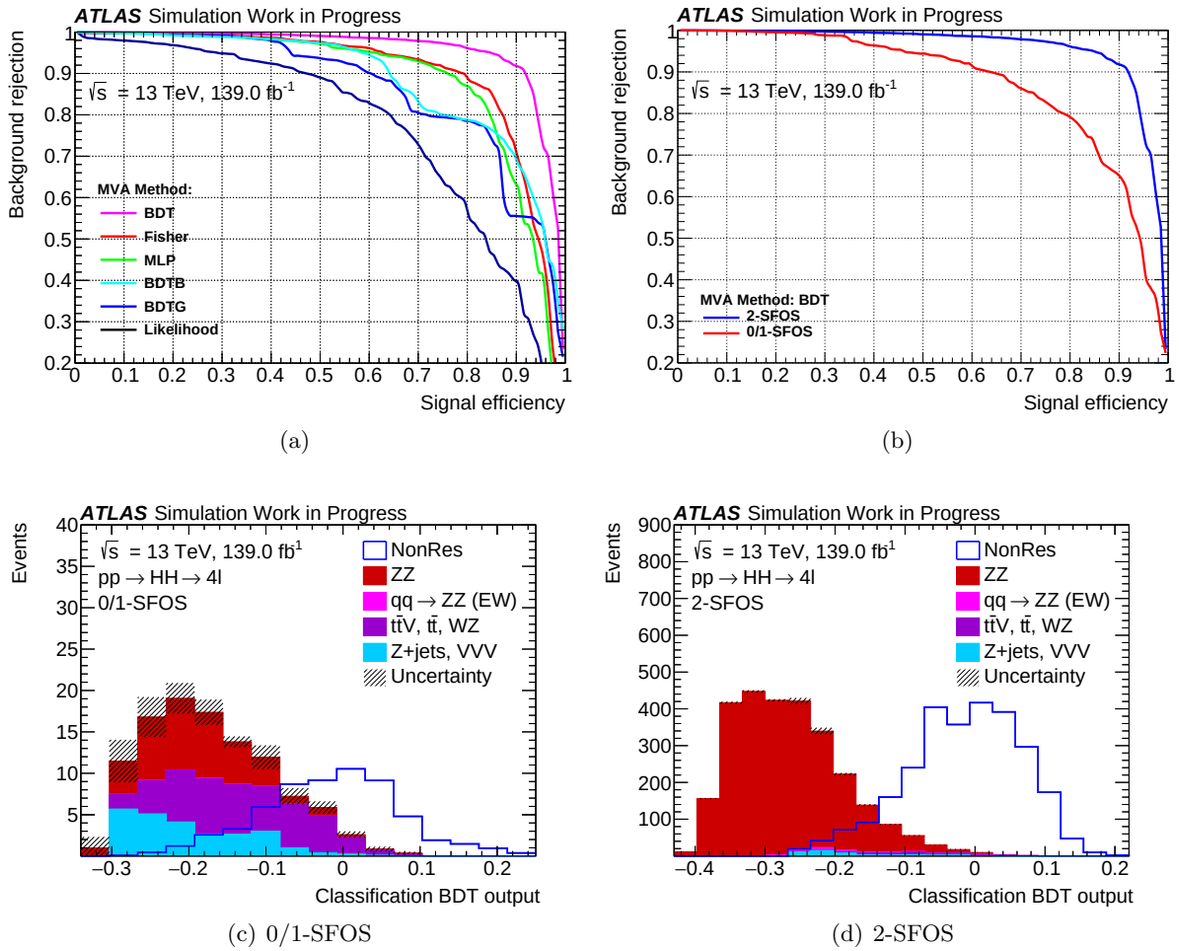

Figure 4. The BDT classification output of the signal and background captured after the training and the resulting weight application. The Receiver operating characteristic (ROC) curve showing the background rejection as a function of the signal efficiency for (a) different MVA algorithms and (b) the BDT for both 2-SFOS and 0/1-SFOS categories.

The area under the curve (AUC) is found to be 95.9% (87.4%) for 2-SFOS (0/1-SFOS). Finally, the classification of the BDT output is shown for 0/1-SFOS and 2-SFOS signal regions in Figures 4(c) and 4(d), respectively.

5. Systematic uncertainties

A global uncertainty of $\pm 1.7\%$ [15] on the total integrated luminosity of the data reported between 2015 and 2018 is considered. In addition, theoretical uncertainties on the signal's cross section are considered. For examples, $\pm 2.1\%$ uncertainty on the PDF and α_S, and $^{+2.2\%}_{-5.0\%}$ from the QCD scale. Other experimental systematic uncertainties are not included in the analysis, like the lepton energy scale and resolution, etc.

6. Statistics and results

Statistical analysis is performed using the profile-likelihood-ratio test statistic [17]. A simultaneous fit on the 0/1-SFOS and 2-SFOS signal regions using background only Asimov data is carried. Since the invariant mass of the 4-lepton is included during the training, the classification BDT output is utilised as a discriminant. A bin transformation method was used

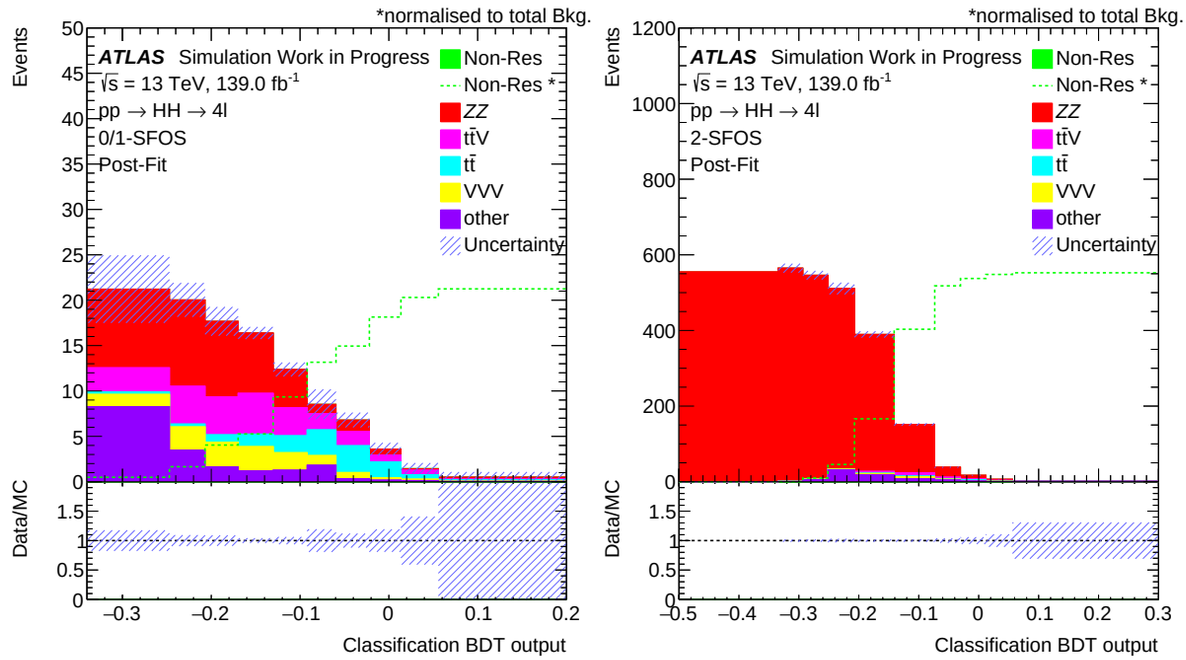

Figure 5. The classification BDT output fitted to background only Asimov data for 0/1-SFOS (left) and 2-SFOS (right) signal regions.

to avoid bins with low statistics. Figure 5 shows the post-fit result after the background only Asimov data fit. The $q\bar{q} \to ZZ$ and $gg \to ZZ$ backgrounds normalisation is set to free during the fit. The CL_s approach is used to set-up an upper limit on the cross-section times the branching ratio of the Higgs pair production. The upper limit is found to be as follows:

$$L^{+1\sigma,+2\sigma}_{-1\sigma,-2\sigma} = 49.22^{+35.4,+72.18}_{-13.75,-22.80}$$

7. Conclusion

A search for the non-resonant SM Higgs pair production via gluon fusion in the four-lepton channel is performed. The data used in the analysis is coming from MC simulation with an integrated luminosity equivalent to 139 fb^{-1}. The expected upper limit at 95% CL_s on cross-section times the non-resonant Higgs pair branching ratio is found to be 49.22 times the SM prediction.

Acknowledgments

Abdualazem Fadol acknowledges the funding support by the CAS-TWAS President's PhD Fellowship Programme.

References

[1] ATLAS Collaboration 2012 *Phys. Lett.* B **716** 1-29 arXiv:1207.7214 [hep-ex]
[2] CMS Collaboration 2012 *Phys. Lett.* B **716** 30-61 arXiv:1207.7235 [hep-ex]
[3] ATLAS Collaboration 2015 *Eur. Phys. J.* C **75** no.10 476 arXiv:1506.05669 [hep-ex]
[4] CMS Collaboration 2015 *Phys. Rev.* D **92** no.1 012004 arXiv:1411.3441 [hep-ex]
[5] ATLAS Collaboration 2019 *JHEP* **05** 124 arXiv:1811.11028 [hep-ex]
[6] Baur U, Plehn T and Rainwater D L 2002 *Phys. Rev. Lett.* **89** 151801–4 arXiv:0206024 [hep-ph]
[7] von Buddenbrock S, Chakrabarty N, Cornell A S, Kar D, Kumar M, Mandal T, Mellado B, Mukhopadhyaya B, Reed R G and Ruan X 2016 *Eur. Phys.* J. C **76** no.10 580 arXiv:1606.01674 [hep-ph]

[8] Alwall J, Herquet M, Maltoni F, Mattelaer O and Stelzer T 2011 *JHEP* **06** 128 arXiv:1106.0522 [hep-ph].
[9] Sjöstrand T, Ask S, Christiansen J R, Corke R, Desai N, Ilten P, Mrenna S, Prestel S, Rasmussen C O and Skands P Z 2015 *Comput. Phys. Commun.* **191** 159 – 177 arXiv:1410.3012 [hep-ph]
[10] Gleisberg T, Hoeche S, Krauss F, Schonherr M, Schumann S, Siegert F and Winter J 2009 *JHEP* **02** 007 arXiv:0811.4622 [hep-ph].
[11] Ball R D *et al* 2015 *JHEP* **04** 040 arXiv:1410.8849 [hep-ph]
[12] Alioli S, Nason P, Oleari C and Re E 2010 *JHEP* **06** 043 arXiv:1002.2581 [hep-ph]
[13] Lange D J 2001 *Nucl. Instrum. Meth.* A **462** 152 – 155
[14] ATLAS Collaboration 2017 *Eur. Phys. J.* C **77** no.5 317 arXiv:1611.09661 [hep-ex]
[15] ATLAS Collaboration 2019 Luminosity determination in pp collisions at $\sqrt{s} = 13$ TeV using the ATLAS detector at the LHC *ATLAS-CONF-2019-021*
[16] Hocker A, Speckmayer P, Stelzer J, Therhaag J, von Toerne E, Voss H, Backes M, Carli T, Cohen O and Christov A 2007 arXiv:physics/0703039 [physics.data-an]
[17] Cowan G, Cranmer K, Gross E and Vitells O 2011 *Eur. Phys.* J. C **71** 1554 Erratum: 2013 *Eur. Phys.* J. C **73** 2501